# Configuration characteristics of the Chinese First Quasi-axisymmetric Stellarator

# Configuration Characteristics of the Chinese First Quasi-axisymmetric Stellarator

Haifeng Liu[1,4*], Akihiro Shimizu[2], Yuhong Xu[1*], Shoichi Okamura[2], Shigeyoshi Kinoshita[2], Mitsutaka Isobe[2,3], Yangbo Li[1], Guozheng Xiong[1], Xianqu Wang[1], Jie Huang[1], Jun Cheng[2], Hai Liu[1], Xin Zhang[1], Dapeng Yin[5], Yi Wan[5], Takanori Murase[2], Sho Nakagawa[2], Changjian Tang[1,4]

[1)] Institute of Fusion Science, School of Physical Science and Technology, Southwest Jiaotong University, Chengdu 610031, China
[2)] National Institute for Fusion Science, National Institutes of Natural Sciences, Toki 509-5292, Japan
[3)] The Graduate University for Advanced Studies (SOKENDAI), Toki 509-5292, Japan
[4)] College of Physics, Sichuan University, Chengdu 610065, China
[5)] Hefei Keye Electro Physical Equipment Manufacturing Co., Ltd, Hefei 230000, China

The Chinese First Quasi-axisymmetric Stellarator (CFQS) will be the first operational quasi-axially symmetric stellarator in the world. The physical and engineering complexities led to the cancellation of two famous quasi-axisymmetric stellarators, CHS-qa and NCSX. Therefore, the major mission of the CFQS is to experimentally achieve the canonical quasi-axisymmetric configuration. The CFQS has been designed to possess a number of advanced features in fixed and free-boundary equilibria. It is a compact stellarator with an aspect ratio R/a ~ 4.0. The neoclassical diffusion coefficient is similar to that of tokamaks in the collisionless regime. The MHD equilibrium of the CFQS configuration is stable up to volume-averaged normalized pressure $\beta$ ~ 1.1%. A region of the second ballooning stability exists in this facility with a large region of plasma, becoming second stable for $\beta$ ~ 2.7% in free-boundary equilibria. The gap between the first and second stability boundaries is very narrow, which is greatly beneficial for the CFQS operation in the second stable regime with high $\beta$ plasma. A modular coil system with 16 coils is designed which robustly reproduces the standard quasi-axisymmetric magnetic field.

## Introduction

In the recent decade, helical systems (stellarators) have made a remarkable progress in magnetic fusion research. In 2015, Wendelstein 7-X at the Greifswald branch of Max Planck Institute for Plasma Physics ignited the first plasma [1], which is the world's largest fusion device of the stellarator type. In the inertially cooled carbon diveror campaign, a new triple product record for stellarators was achieved, $n\tau_E T_i = 6.81019\times10^{19}$ keVm$^{-3}$s in 2017 [2]. Besides it, important studies were conducted concerning the magnetic island divertor, which is instrumental for achieving long-pulse or steady-state operations [3]. In the same year, the deuterium plasma experiments had been executed successfully on the Large Helical Device (LHD). One of the significant achievements is that ion temperature reaches the 10 keV [4]. The isotope effect on energy confinement time and thermal transport has been investigated and hydrogen and deuterium plasmas heated by neutral beam injection have exhibited no significant dependence on the isotope mass in thermal energy confinement time, which is not consistent with the simple gyro-Bohm model [5,6]. In 2017 Southwest Jiaotong University (SWJTU) in China and National Institute for Fusion Science (NIFS) in Japan signed an

official agreement to design and operate collaboratively the CFQS [7-9]. Advanced configuration design studies of stellarator facilities have also been developed greatly owing to the great freedom in the geometry of three-dimensional (3D) helical system structures e.g. the quasi-symmetric configuration and quasi-isodynamic configuration [10,11]. In such new configuration developments, the primary objectives are to improve neoclassical transport and explore high-$\beta$ configurations [12,13]. As for quasi-symmetric configurations, there are three characteristic types of magnetic topologies, quasi-helical symmetry, quasi-axisymmetry and quasi-poloidal symmetry [14,15]. The first experimental test of the quasi-symmetry is the Helically Symmetric eXperiment (HSX), operating at the University of Wisconsin [16].

Quasi-axisymmetric stellarators (QAS), i.e. stellarators with |B| symmetric in the toroidal (Boozer) direction [17], would have neoclassical transport very similar to that of tokamaks while keeping intrinsic advantages of stellarators, such as the absence of disruptions [18,19]. Using the 3D shaping freedom available in a stellarator, configurations can be designed that are MHD stable without nearby conducting structure, requiring no current drive at high $\beta$. Moreover, the reduced damping of toroidal rotations leads to improved confinement through plasma sheared rotations [19]. Quasi-axisymmetric plasmas have a similar level of the neoclassical bootstrap current to tokamaks [21,22]. The increase of the rotational transform of high $\beta$ plasmas may contribute to better MHD properties and confinement. The rotational transform profile produced by the 3D shaping and neoclassical bootstrap current can be designed to monotonically increase towards the plasma edge, like the core region of a 'reversed shear' advanced tokamak, which is utilized to stabilize neoclassical tearing modes, reduce equilibrium islands, and stabilize trapped-particle driven modes [23]. In addition, low aspect ratio achieved in the quasi-axisymmetric configuration is attractive in order to minimize the cost of fusion experiments and the capital cost of possible future power plants. NCSX [24, 25] and CHS-qa [19, 21] were typically quasi-axisymmetric stellarators. Main parameters for the NCSX are major radius R= 1.4 m, magnetic field strength Bt = 2.0 T and aspect ratio Ap = 4.4 and for CHS-qa are R=1.5 m, Bt = 1.5 T and Ap = 3.2, respectively. The large device size and high magnetic field strength would considerably increase fabrication cost which partly led these two stellarators not to be completely constructed. In addition, high accuracy requirement on modular coils was the large driver of cost growth and therefore, any advances in stellarator coil optimization can potentially bring remarkable impact on the practicability of magnetic confined fusion devices. Based on their experiences, via the scan of the major radius (1.0 m-1.5 m) and aspect ratio (3-5), we investigated a number of configurations and finally obtained the desirable one characterized by R=1.0m, Bt=1.0T and Ap=4.0, respectively [7-9]. The device size and magnetic field strength for the CFQS are smaller than these for the NCSX and CHS-qa. The toroidal periodic number N = 2 is chosen for the better achievement of the quasi-axisymmetry. With respect to further optimizations of coils we found that the surface torsions of finite-sized coils are greatly influential on the simplification of modular coils and fabrication accuracy. We have figured out how to design a surface-torsion-free coil system and a set of practical coils without surface torsions was accomplished for the CFQS [26]. The surface torsions merely exist in finite-sized coils rather than filament coils. To date all coil-design codes, e.g. NESCOIL, COILOPT, FOUCS codes [27-29], etc.,

almost primarily attribute to optimization of filament coils for stellarators without considering finite-size effects.

Concerning future CFQS experiments, two types of discharge operations, i.e., the plasma-current-free and bootstrap-current-carrying scenarios, will be implemented. In this paper, we just focus on the plasma-current-free scenario in the CFQS and discuss advanced configuration characteristics and design of the coil system for the CFQS. The electron cyclotron current drive (ECCD) is being explored as an option control the net toroidal current in W7-X [30,31], which is also expected to be applied to suppression of the bootstrap current in CFQS.

## 2. CFQS configuration and filament modular coils

The CFQS is designed as a laboratory-scale stellarator. It would be the first facility to explore confinement properties of quasi-axisymmetric magnetic configurations. One of the primary fabrication aims is the accomplishment of the reduction of neoclassic transport in a tokamak-like environment and with absence of disruptions. The entire physical design of the CFQS consists of two aspects: the magnetic configuration design and coil system design. Concerning the former, we consider early design experiences of QAS are important for the CFQS fabrication, because to date any other QAS cannot be realized successfully for various reasons in the world. To efficiently accelerate and finalize physics design work, the CFQS configuration was designed based on the CHS-qa [19, 21]. This device had a number of the advanced QA configuration properties, which was optimized by reducing the non-axisymmetric components of the Boozer spectra, controlling the rotational transform bounded within the assumed range of values, avoiding low order rational flux surfaces and stabilization of ballooning and Mercier modes [19]. The more detailed design strategies were shown in the references [7-9]. Concerning the latter, the Ap=4.0 selected is the most compact in the operational stellarators with modular coils. Therefore, it is of great challenge to design a modular coil system for the CFQS. Via consideration of the realization of the target magnetic configuration, the complexity of coil shapes and coil-coil intervals, a set of filament coils was designed successfully and comprises 16 modular coils by NESCOIL code [7]. The MHD equilibria were performed by the VMEC code [32] with poloidal mode number = 8, toroidal mode number = 4, number of flux surfaces = 61, etc. The three-dimensional magnetic field strength can be expanded in the Boozer coordinates with a form of Fourier series:

$$B(\psi,\theta_B,\phi_B)=\sum_{m,n}(B_{mn}(\psi)\cos(m\theta_B-nN\phi_B)) \quad (1)$$

Where the coefficients $B_{\mathrm{mn}}$ are referred to as the spectrum of the magnetic field strength. The $\psi$, $\theta_B$ and $\phi_B$ form spatial Boozer coordinates.

Fig.1 displays the objective plasma boundary with nested magnetic flux surfaces at three different toroidal angles. These surfaces indicate large toroidal-averaged crescent, elongation and triangularity, which is positive for stabilities of ballooning and kink modes. The crescent and triangularity of the plasma shape mainly associate with two Fourier components with m=1, n=0 and m=2, n=0, which are the first and fourth dominant

components. The elongation is mainly shaped by the largest non-symmetric component with m=1, n=1. This component also contributes to the rotational transform of magnetic fields by twisted elongations as well as a helical excursion of the magnetic axis. In Fig. 2(a) ploted is the Fourier spetrum of the magnetic field strength nomalized to $B_{0,0}$ in the Boozer coordinates in the plasma pressure-free configuration. The dominant component is the $B_{1,0}$ which guarantees achievement of the quasi-axial symmetry. In Fig.2(b), it gives the rotational transform and depth of the magnetic well versus the nomalized magetic flux. A flat iota profile is beneficial to sustain the internal transport barrier [33] and the magnetic well structure exists in the global plasma region which enables MHD stabilities.

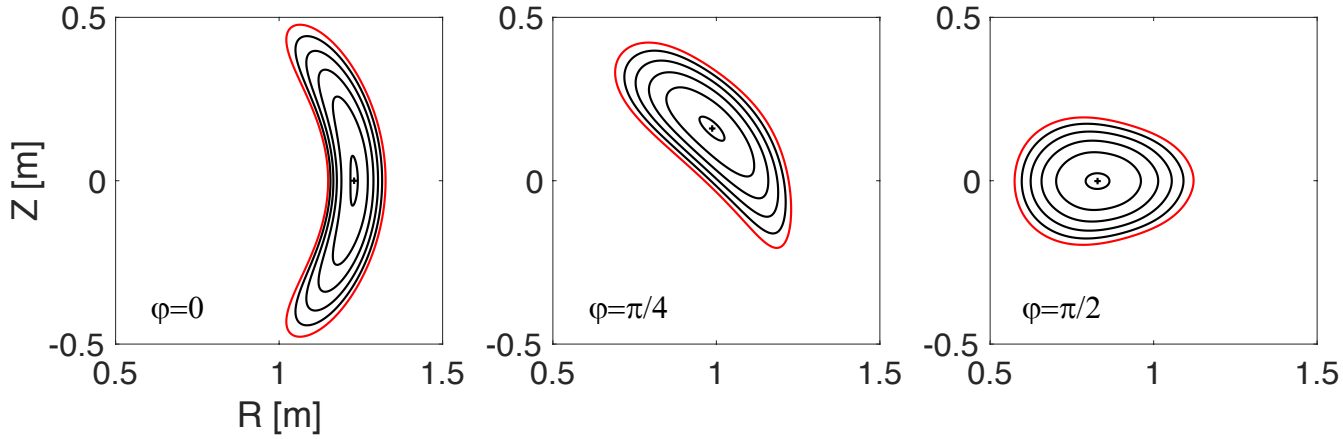


Figure.1 Shape of the target plasma boundary with magnetic flux surfaces for the vacuumed CFQS configuration at three different toroidal angles

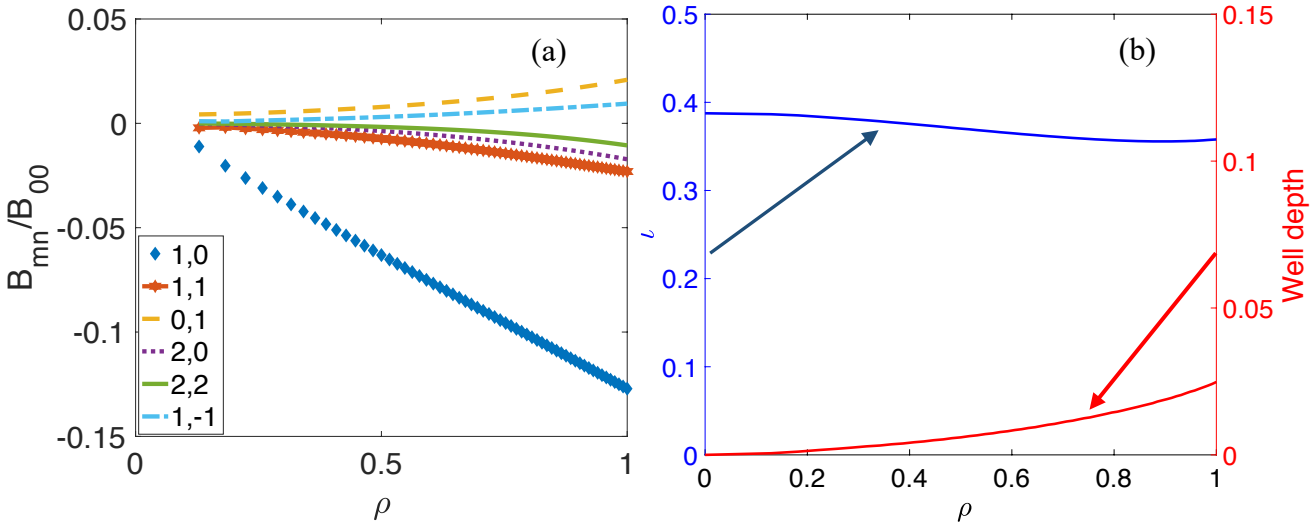


Figure.2 Magnetic field strength spectra normalized by $B_{0,0}$ in the Boozer coordinates for the CFQS configuration without plasmas (a) and the rotational transform and magnetic well depth in this configuration (b).

In order to achieve the target magnetic configuration, a filament coil system has been designed to reproduce the plasma boundary. Fig.3 gives the modular coil system with 16 non-planar coils which can closely generate the objective magnetic configuration, which was revealed in our previous work [7]. Due to the toroidal periodicity = 2 and stellarator symmetry, the whole torus consists of four symmetric sections. Therefore, the coil system possesses four different shaped modular coils (MC1-MC4). This filament coil design is finalized

with the NESCOIL code which was also executed to develop coil systems for the W7-x, NCSX and CHS-qa [34-36]. In the section 3 the 16 filament coils will be utilized to estimate CFQS configuration preparties in free-boundary equilibria.

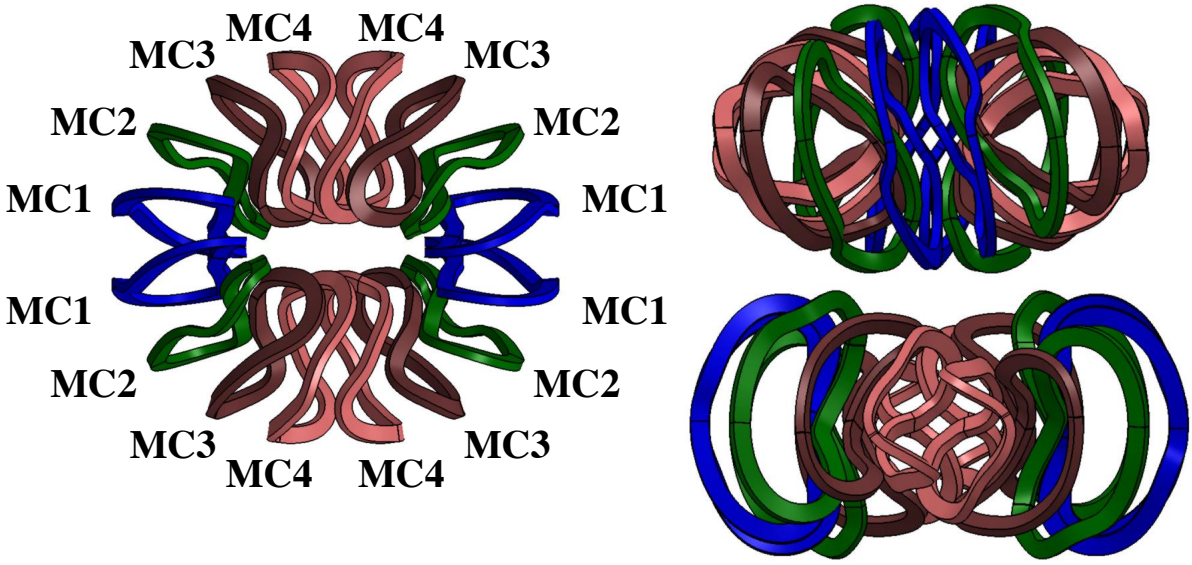


Figure.3 Modular coils of the CFQS, the top view and side views at toroidal angle = $0^\circ$ (vertical elongation), and $90^\circ$ (horizontal elongation). The serial numbers (MC1-MC4) of coils represent the various shapes of coils. The coil system comprises of four different shape coils.

Three different routes to produce a magnetic field rotational transform were proved mathematically by Spitzer and Mercier [37, 38], which are through driving a toroidal current, by rotating elongated magnetic flux surfaces poloidally and by making the magnetic axis non-planar. They give the expression of the rotational transform as an itergral along the magneic axis, as follows

$$\iota = \frac{1}{2\pi}\int_0^L [\frac{\mu_0 J}{2B_0} - (\cosh\eta - 1)d' - \tau]\frac{dl}{\cosh\eta} - N. \quad (2)$$

Where $J$ is the current density on the magnetic axis, $N$ is an integer of the topological origin, $\eta = \ln(r_2/r_1)$ the elongation of the flux surfaces, $d$ tilting angle with respect to the curvature and $\tau$ denotes its torsion. Tokamaks and reversed field pinches utilize the first route and LHD utilizes the second one, TJ-II, Heliotron J and Wendelstein 7-X the latter two. Recently the last route turns more and more important and is applied to design a new class of stellarators with a magnetic axis in the shape of a knot, e.g., "knotatrons" [39, 40], which has a large volume filled with closed magnetic surfaces, with significant rotational-transform, and with the magnetic field produced entirely by external circular coils.

In the CFQS, these three routes are all employed for the generation of the magnetic field rotational transform. Fig 4 shows the shapes of the magnetic surfaces near the magnetic axis at 6 toroidal locations. Black spots at the center of magnetic flux surfaces describe the corresponding locations of the magnetic axis. The magnetic axis is non-planar and the elliptical flux surfaces rotate along toroidal angles, which makes magnetic field lines twisted poloidally. Meanwhile, the bootstrap current is sizably high in the CFQS [8] and also increase

the rotational transform. When the $\beta$ increases to 1.5%, the neoclassical bootstrap current approaches 32kA and from the core region to the edge the rotational transform grows to 3/7 and 3/5.

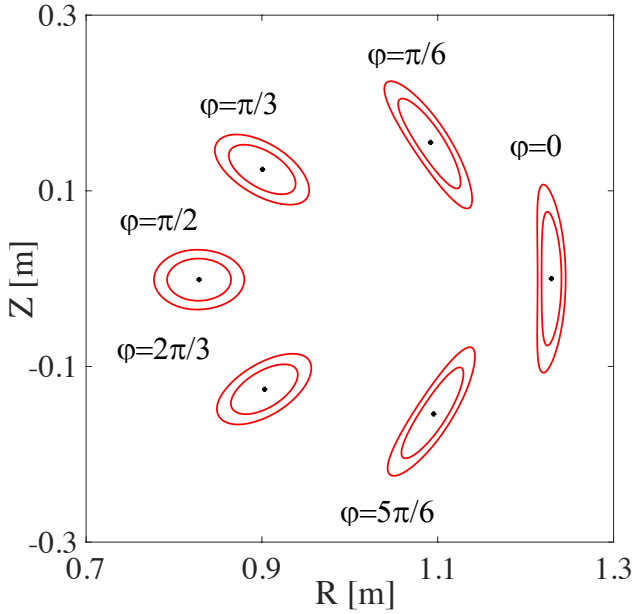


Figure. 4 the shapes of the magnetic surfaces in the vicinity of the magnetic axis at 6 toroidal locations, and black cross-shaped spots are the corresponding locations of the magnetic axis.

## 3. Configuration preparties in fixed and free-boundary equilibria

In Figs. 5(a)-(c) contours of magnetic field strength at ρ=0.5 are displayed for fixed boundary equilibria with β=0%, β=2.0% and free boundary equilibrium with β=2.0%, respectively. In the Boozer coordinates the corresponding magnetic field strength spectra with n ≠0 and $B_{2,0}$ modes normalized by $B_{0,0}$ are given in Figs. 5(d)-(f). It is shown that when $\beta$ is inceeased to 2.0%, although the magnetic flux surfaces are deformed the propertis of the quasi-axisymmetry are sustained in fixed and free boundary equlibria in Figs. 5(e)-(f). In comparison with the Fourier spectra of the magnetic field strength in the vacuum equilibrium in Fig. 5(d), the amplitude of the toroidal symmetric compomnent $B_{2,0}$ is incresed siginificantly and supresses the subdominant non-symmetric $B_{1,1}$ as shown in Fig. 5(e)-(f), which plays an essential role on the ballooning stabilities duo to three- dimensional magnetic surface reshaping [41]. The bumpy field $B_{0,8}$ is induced by discrete coils shown in Fig. 5(f), which doesn't significantly enhance neoclassical transport as displayed in Fig. 7. The comparison of the rotational transform and magnetic well for fixed ($\beta$=0.0%, $\beta$=2.0%) and free ($\beta$=2.0%) boundary equilibria is depicted in Figs. 6. As $\beta$ inceeases the rotational transform is slightly decreased duo to the deformations of magnetic surface shapes. Meanwhile, the structure of the magnetic well is sustained and intensified integrally, which advantageously makes Mercier modes stabile in high $\beta$ plasmas.

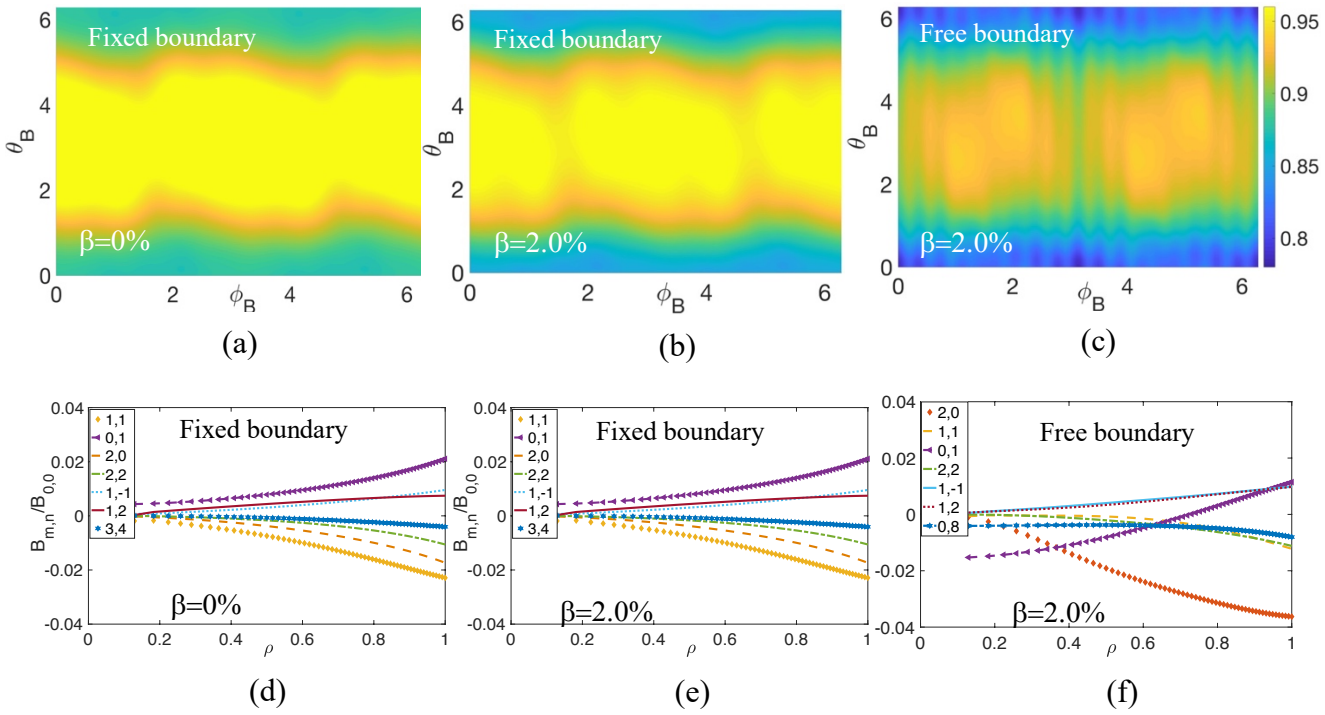


Figure.5 Magnetic field strength contours at ρ=0.5 for fixed boundary equilibria with $\beta$=0% (a), $\beta$=2.0% (b) and free boundary equilibrium with $\beta$=2.0% (c), respectively; Magnetic field strength spectra with $n \neq 0$ and $B_{2,0}$ modes normalized by $B_{0,0}$ in the Boozer coordinates for these corresponding equilibria on the second row.

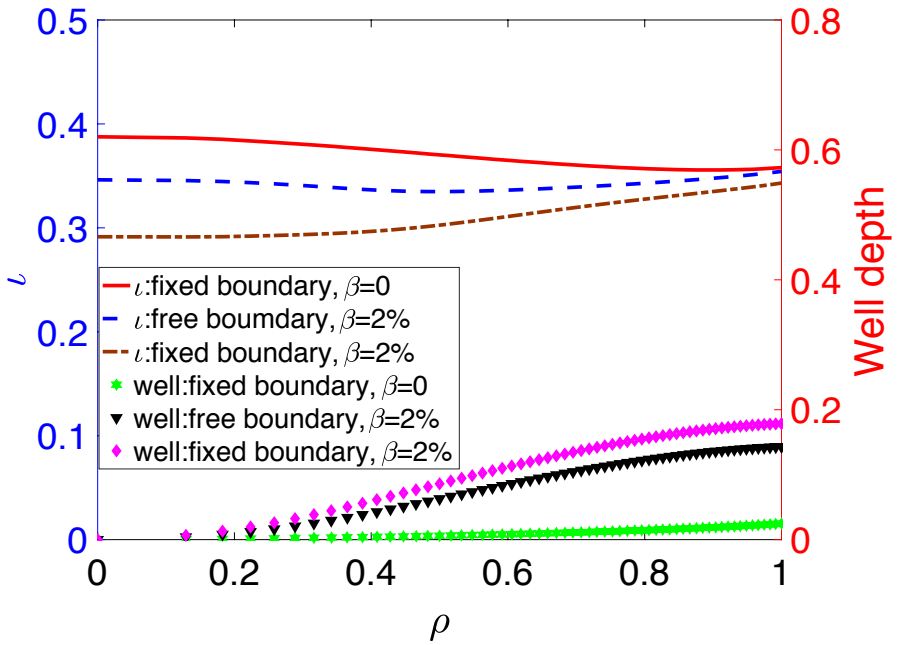


Figure.6 The rotational transform profiles for the fixed boundary equilibrium without plasma (red solid curve), free boundary equilibrium with β=2.0% (blue dashed curve), fixed boundary equilibrium with β=2.0% (yellow dash dot curve), respectively; magnetic well depth profiles for the fixed boundary equilibrium without plasma (bright green asterisks), free boundary equilibrium with β=2.0% (black triangles), fixed boundary equilibrium with β=2.0% (pink diamonds), respectively.

In the CFQS configuration, the pseudo-axisymmetry target has been developed which directly minimize helical and toroidal ripples in the Boozer coordinate space. It achieves a tokamak-like neoclassical transport level. The estimation of the neoclassical transport can be characterized by the effective ripple strength $\varepsilon_{eff}$ [42]. The neoclassical diffusion coefficient $D_{neo}$ is expressed as follows:

$$D_{neo} \propto \frac{\varepsilon_{eff}^{3/2} v_d^2}{\nu} \quad (2)$$

Where $v_d$ *and* $\nu$ donate the radial drift velocity and collision frequency. The radial profiles of $\varepsilon_{eff}^{3/2}$ calculated by the NEO code [42] are displayed in Fig. 7. The number of mesh points in poloidal and toroidal directions is 200×200. 75 test trapped particles are initialized to estimate this performance. The parabolic plasma pressure is assumed. These figures show the radial profiles for the free and fixed boundary equilibria with various $\beta$ in Figs. 7(b) and (c), respectively. As comparison with the CFQS, the CHS [43, 44] is under consideration and the $\varepsilon_{eff}^{3/2}$ profile of the CHS in the fixed boundary is given as well. The $\varepsilon_{eff}^{3/2}$ of the CFQS is much lower than that of CHS, approximately three orders lower. In addition, the enhanced confinement property of the neoclassical transport is robust as $\beta$ increases in fixed and free boundary equilibria because the quasi-axisymmetry property is favorably sustained with enhancement of $B_{2,0}$ in Figs. 5(e) and (f). Concerning free boundary equilibria, the coil-induced mirror ripples in Fig.5 (c) do not significantly give rise to the increase of neoclassical transport. This code is also used to evaluate neoclassical transport properties in LHD, CHS-qa, W7-x et.al [45-47] and optimization of stellarotors [15]. Generally, in comparison with quasi-isodynamic and quasi-helical configurations, the neoclassical transport in QAs is lower when other device parameters are similar.

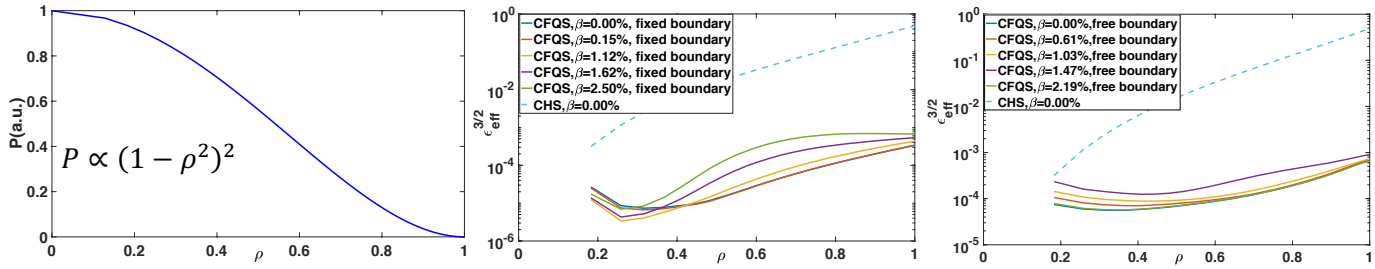


(a) (b) (c)

Figure. 7 (a) assumed pressure profile, $P \propto (1-\rho^2)^2$; radial profiles of the effective helical ripple of the CFQS for fixed (b) and free (c) boundary equilibria. The result of the CHS is referred, plotted by a blue dashed curve.

The stabilities of Mercier and ballooning modes are estimated by the VMEC and COBRAVMEC codes [48] in the free and fixed boundary conditions. The Mercier criterion for the stability is given by $D_{merc}=D_{shear}+D_{well}+D_{curr}+D_{geod}>0$ where they represent magnetic shear term, magnetic well term, current term and geodesic couverture term, respectively. At three different radial positions, the variation of Mercier stabilities with the volume-averaged $\beta$ is given in Fig.8(a) for the fixed boundary and Fig.8(c) for the free boundary, which illustrates that the interchange mode is stable up to $\beta$=2.0%. In the CFQS, the robustness of the magnetic well is sustained as the $\beta$ increases in Fig. (6), which enables to overwhelm the destabilization effect of the geodesic curvature and make interchange modes stabilized displayed in Figs.8(b) and (d).

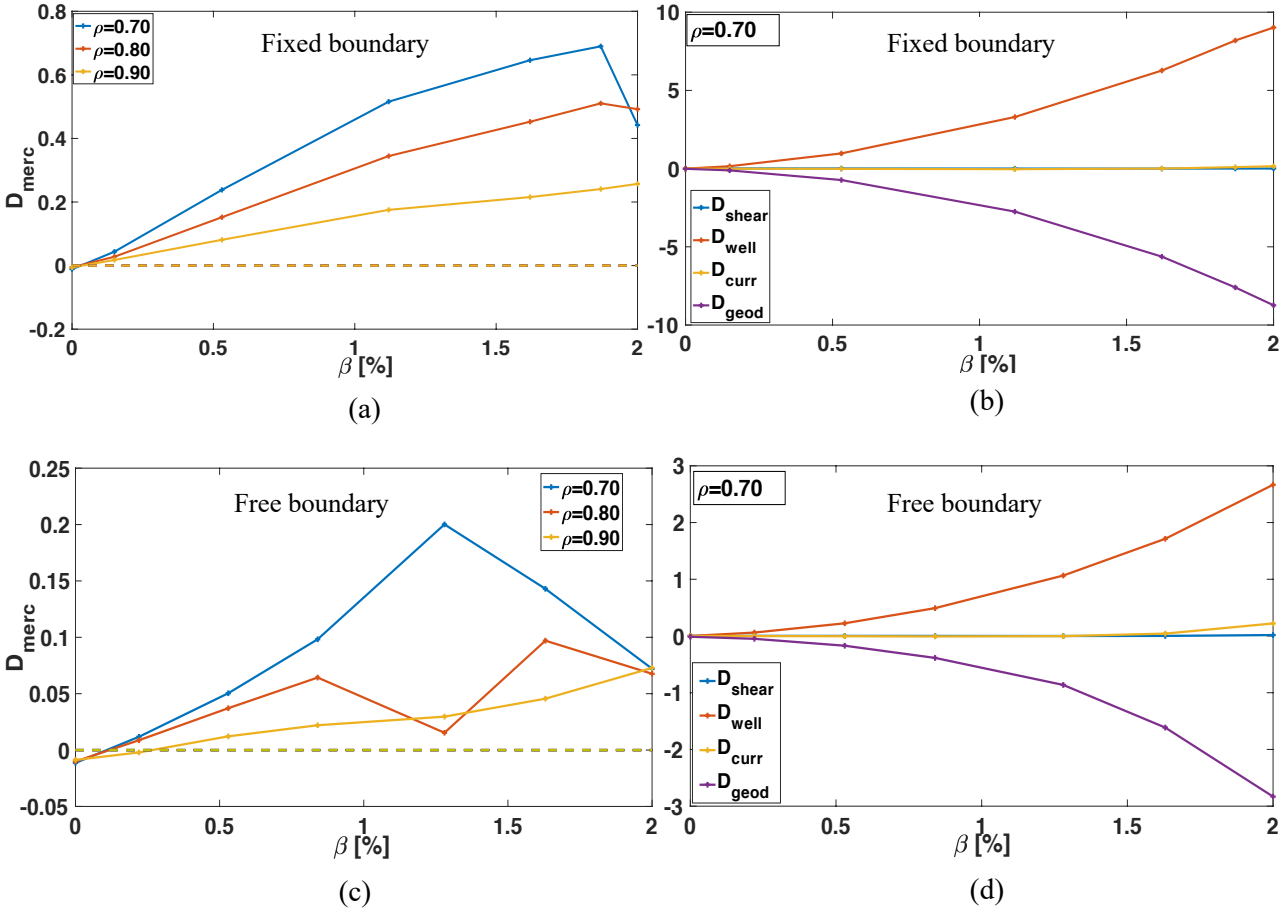


Figure. 8 Mercier stabilities versus $\beta$ in the fixed boundary (a) and free boundary (c) at three different radial positions ρ=0.7, 0.8 and 0.9 respectively; magnetic shear term, magnetic well term, current term and geodesic couverture term versus $\beta$ in the fixed boundary (b) and free boundary (d) at ρ=0.7.

The COBRAVMEC code solves for the most unstable ballooning mode on a given surface using Richardson extrapolation in VMEC coordinates. This code calculates the local (on a field line) ballooning growth rate with the infinite-n ballooning mode limit. All of the infinite-n ballooning stability results shown in Fig. 9. The second ballooning stability is able to steadily exist in the CFQS device. Ballooning growth rates as a function of the normalized flux ρ in the first stability region are displayed in Fig. 9(a) for the free boundary. As the plasma pressure is increased, the plasma first becomes unstable at $\beta$ =1.1%. The region of ballooning instabilities grows until $\beta$ =2.7%, where a region of the second stability appears as shown in Fig. 9(b). From $\beta$ =2.7%-3.6%, the second stability is sustained. In the second stable region the amplitude of $B_{2,0}$ is greatly enlarged as $\beta$ increases shown in Fig.5(e). This provides a strong component of the triangularity. The enhancement of the toroidal symmetry component in the local shear of the quasi-symmetric configuration can increase ideal MHD stability threshold conditions and give rise to second stability regimes [41]. The ballooning modes are less localized in regions of unfavourable stelarator-like curvatures, and so are more sensitive to the stabilizing effects of the average curvature. Thus, the ballooning modes can be utterly stabilized at sufficiently low global shear in the CFQS. Futhermore, it is noted that the gap between the first and second stability $\beta$ ~1.1%-2.7% is much narrower than that in the quasi-poloidal stellarator configurations [49]. The similar result is also obtained in the fixed boundary equilibria in Figs.9(c) and (d). The implications for the possibility of operating the CFQS at the second instable region are more achievable. The stabilization

of Mercier and ballooning modes is essential to achieve a high β plasma which is usually considered in optimization of stellarator configurations [15, 18, 21]. Notably, high-β equilibria of drift-optimized compact stellarators have been obtained with VMEC and COBRAVMEC codes. These configurations have strong magnetic wells and consequently high interchange stability limits up to β= 23%, [50]. Additionally, it should be pointed out that all codes, VMEC, NESCOIL, NEO and COBRAVMEC, which are utilized to estimate the configuration characteristics of CFQS in this paper, are contained in the STELLOPT package [13].

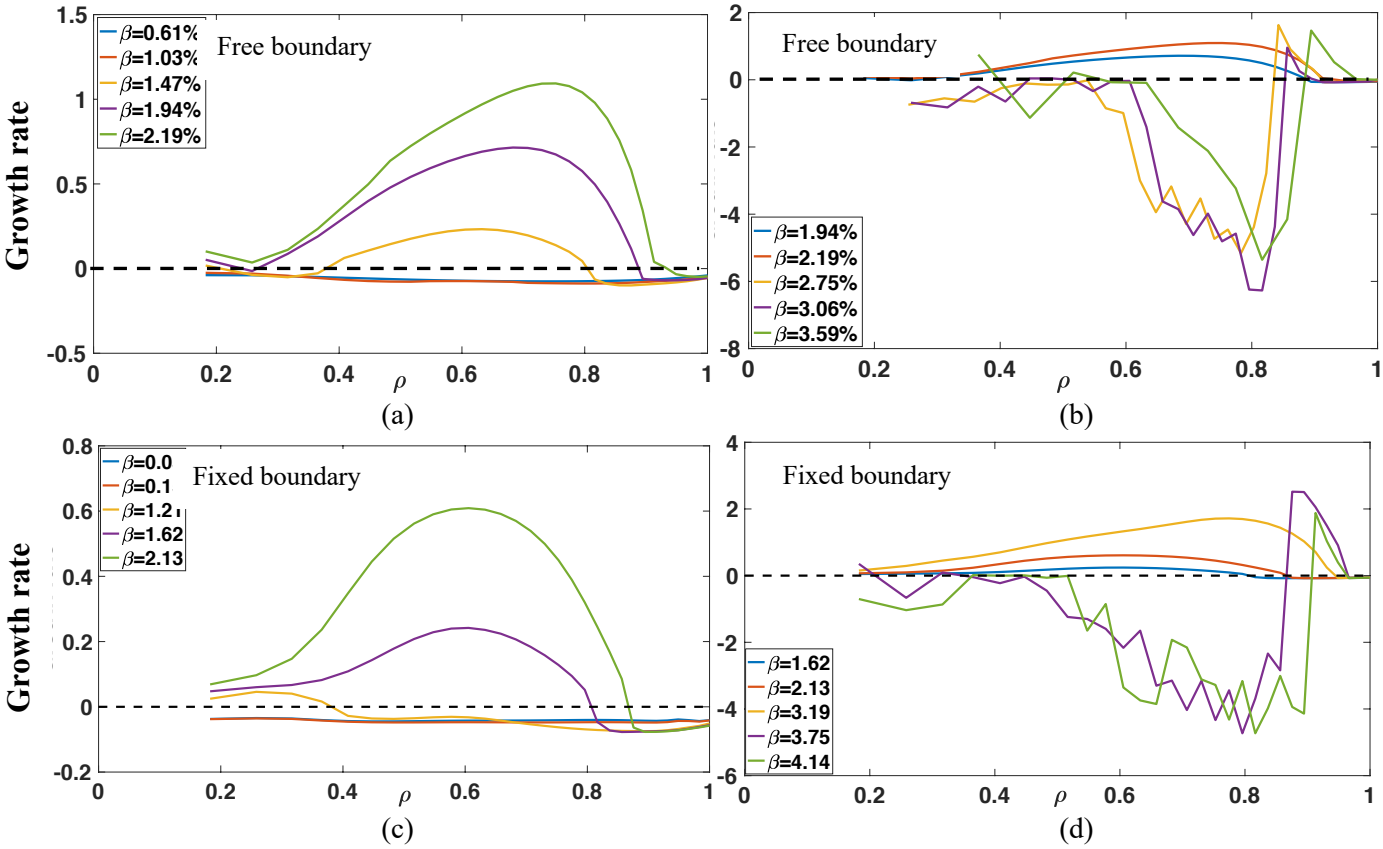


Figure. 9 First stability regions of ballooning modes from the COBRAVMEC code in the free boundary (a) and fixed boundary (c), second stability regions in the free boundary (b) and fixed boundary (d).

In addition to the standard quasi-axisymmetric configuration shown in Fig. 1, the island bundle divertor (IBD) configuration can be also achieved without breaking the quasi-axisymmetry in the core confinement region by adding a weak toroidal field to the quasi-axisymmetry, displayed in Fig.10. This configuration has been designed by S. Okamura, et.al [51]. The confinement region is bounded by an island bundle with ι=2/5, which determines the last closed flux surface (LCFS). The low and flat iota configuration is well-suited for island divertor studies for numerous reasons. First, the edge island chain does not resonate with n=1 error fields, making it less vulnerable to asymmetric deformations that give rise to generation of the stochastic layer [52]. Furthermore, the field lines in the SOL have longer connection lengths compared to the standard CFQS configuration, which would tend to elevate the influence of perpendicular drifts in the edge relative to parallel transport and decentralize ion depositions on divertor plates [53]. The islands exist naturally in the vacuum magnetic field and arise from resonant radial field components generated by the non-planar magnetic field coils. Compared with tokamak divertors [54-56], the CFQS divertors are also significantly different including

(1) that the x-points wrap helically around LCFS and (2) that the divertor targets are toroidally localized, i.e. there exist poloidal cross-sections that do not intersect any divertor targets. In the W7-x the similar divertor configuration (5/5) has been experimentally achieved with excellent performances [2, 52, 53]. In such configuration the highest triple product was approached in stellarators to date.

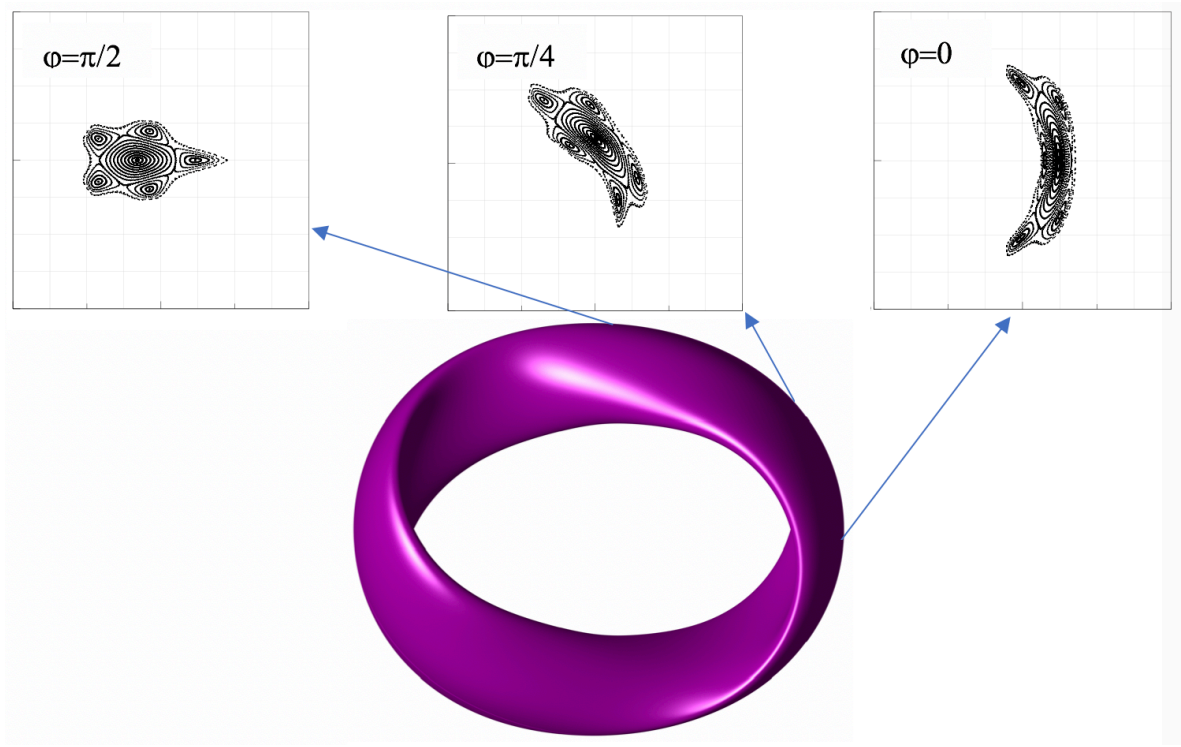


Figure. 10. Geometry of the plasma contour (last closed flux surface) is shown. The three poloidal cross sections at key toroidal angles referred to in this paper, covering an angular range of π/2. On the top shown are closed magnetic flux surfaces and the 2/5 magnetic islands (representing the Poincare plots of the magnetic field lines on these surfaces), including a distinct island separatrix.

CFQS is expected to be operated in two different heating regimes. The facility will be equipped with 1.0 MW of ECRH (54.5 GHz, on axis heating). A low density, high electron temperature case could be achieved. To analyze plasma confinement and MHD behaviors in the second ballooning stable scenario, the impact of 1.0 MW of NBI (tangential injection with beam energy ~ 40 keV) and 2 MW of ICRH which is available in the 40–80 MHz range, has also been considered. This would allow access to higher density regimes than ECRH (density cut-off limited). The operational parameters of CFQS were estimated using the ISS95 scaling law [57]. The radial density and temperature profiles are assumed as $T = T_0(1-\rho^2)$ and $n_e = n_{e0}(1-0.8\rho^2+1.3\rho^4-1.5\rho^6)$, respectively. $T_{i0} = 2/3T_{e0}$. The enhancement factor $H_f$= 1.0, 2.0, 2.5 and 2.9 are under consideration. The line-averaged density is 1 x $10^{19}$ $m^{-3}$ for low-density plasma heating and 4 x $10^{19}$ $m^{-3}$ for high-density plasma heating, respectively. The $H_f$= 2.9 is similar to that in the NCSX [15]. For the B=1.0 T operation, the $\beta$ and $T_{e0}$ variations vs heating power in these two heating regimes are shown in Fig. 11. Concerning the low-density plasma heating the expected $\beta$ ranged from 0.5% to 1.5% at a heating power of 1.0 MW ECRH and the $T_{e0}$ ranged from 1.0 to 3.0 keV as shown in Figs.11(a) and (b). With respect to the high-density plasma heating, the expected $\beta$ ranged from 1.7% to 4.7% with the range of $T_{e0}$ from 0.7 to 2.3

keV at a heating power of 3.0 MW (1.0 MW NBI + 2.0 MW ICRH) as shown in Figs.11(c) and (d). There are numerous reasons to expect that the confinement may be enhanced in the CFQS configuration, compared with conventional stellarators and tokamaks. The robustness of quasisymmetry should reduce neoclassical transport and suppress neoclassical toroidal viscosity, allowing development of persistent zonal flows. Furthermore, the shallow reversed/flat shear could stabilize trapped-particle modes, similar to reversed-shear advanced tokamak regimes.

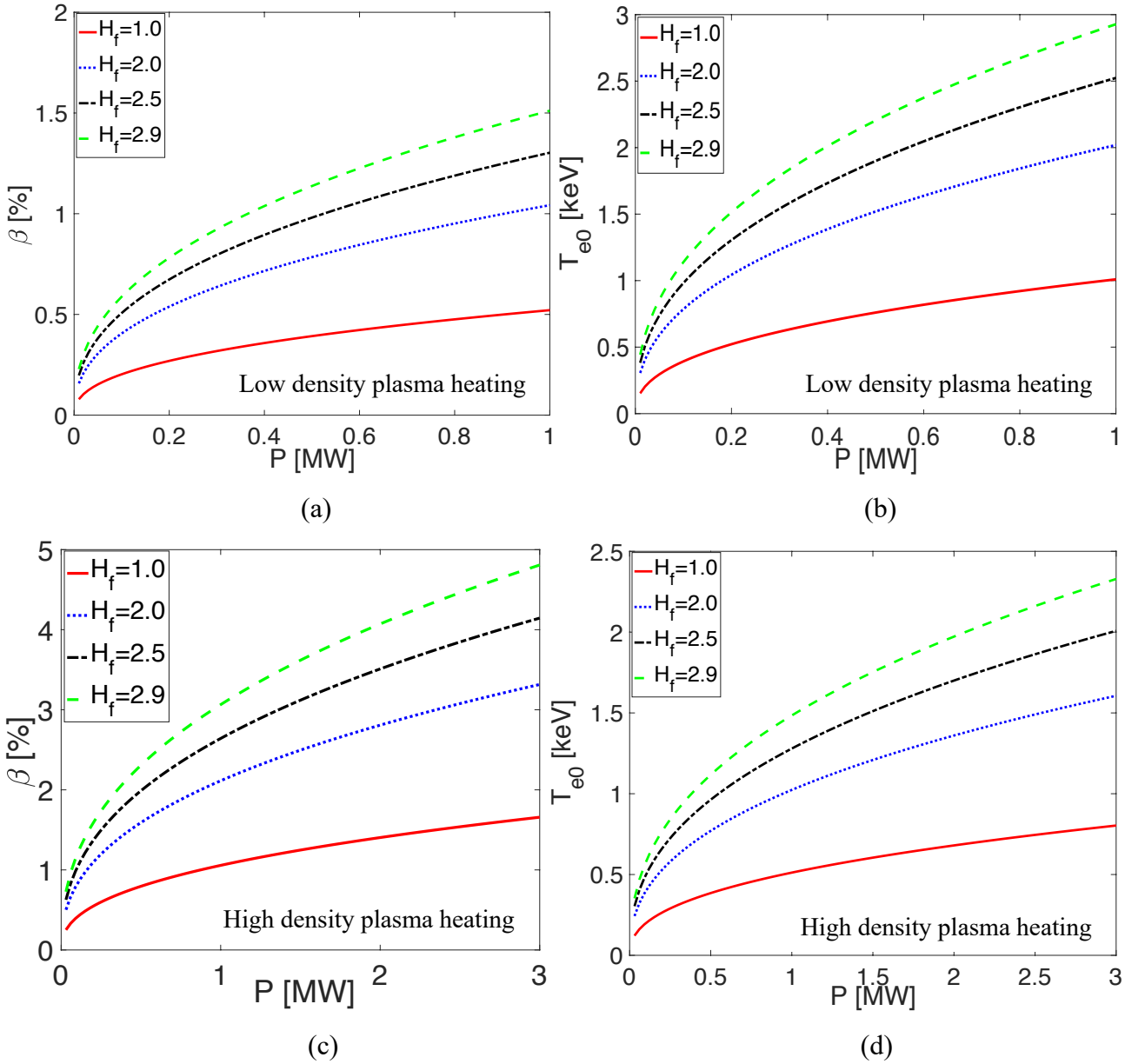


Figure. 11. Volume-averaged β (a) and electron temperature (b) for the low-density plasma heating, (c) and (d) for the high-density plasma heating estimated by the ISS95 scaling law in the B=1.0 T operation.

## 4. Conclusion and future work

A new compact quasi-axisymmetric stellarator configuration has been devised for the CFQS which consists of plenty of favorable features. It compatibly combines characteristics from optimized stellarators and advanced tokamaks, providing a possible access to steady-state reactors without current drive or disruptions. It was found by optimizations of the shape of the plasma boundary, the rotational transform, the magnetic

well, and the quasi-axisymmetric field errors. The Mercier modes are positively stabilized at $\beta$ =2.0%. The first and second regions of stability against ballooning behaviors are shown clearly in Fig. (9). This is accomplished through axisymmetric reshaping. The neoclassical transport coefficients are much lower than in conventional stellarators, nearly the same as that in tokamaks. The IBD configuration can be also achieved without breaking the quasi-axisymmetry in the core confinement region. A modular coil system with 16 non-planar coils consists of four different coil shapes, which precisely realizes the target quasi-axisymmetric configuration.

In future work, the finite-size effect of coils is crucial to magnetic configurations and not avoidable. We are going to implement the surface-torsion analysis for the estimation of stochastic deviations of practical coils during fabrication and assembly of the coil system. Furthermore, how to reduce the gap between the first and second stability boundaries is another interesting topic.

## Acknowledgments

This work was partly supported by the National Natural Science Foundation of China under Grant No. 11820101004, National Key R&D Program of China under Grant Nos. 2017YFE0301705 and 2017YFE0300402 and NIFS General Collaboration Project budget under Grant Nos. NIFS17KBAP034 and NIFS18KBAP041.

## Referances

[1] Clery D. 2015 *Science*
[2] Wolf R. C. 2019 *Phys. Plasmas* **26** 082504
[3] Gao Y. 2019 *Nucl. Fusion* **59** 106015
[4] Osakabe M. 2017 *Fusion Technol.* **1080** 1335145
[5] Yamada H. 2019 *Phys. Rev. Lett.* **123** 185001
[6] Ogawa K., Isobe M. 2019 *Nucl. Fusion* **59** 076017
[7] Liu H. *et al* 2018 *Plasma Fusion Res.* **13** 3405067
[8] Akihiro S. *et al* 2018 *Plasma Fusion Res.* **13** 3403123
[9] Isobe M. *et al* 2019 *Plasma Fusion Res.* **14** 3402074
[10] Kovrizhnykh L.M. 1985 *Nucl. Fusion* **25** 1391-97
[11] Garren D.A. *et al* 1991 *Phys. Fluids* **3** 2822-34
[12] Nührenberg J. 2009 *Phys. Rev. Lett.* **102** 235001
[13] Spong D. *et al* 2001 *Nucl. Fusion* **41** 711
[14] Strickler D.J., Hirshman S.P., Spong D.A. *et al* 2004 *Fusion Sci. Technol.* **45(1)**:15-26.
[15] Zarnstorff M.C. *et al* 2001 *Plasma Phys. Control. Fusion* **43** A237-49
[16] Anderson D.T. *et al* 1994 *Nucl. Fusion* **34** 881-85
[17] Boozer A.H. *et al* 1980 *Phys. Fluids* **23** 904-08
[18] Matsuoka K. *et al* 1997 *Plasma Phys. Rep.* **23** 542-46
[19] Okamura S. *et al* 2001 *Nucl. Fusion* **41** 1865-72
[20] Rosenbluth M.N. *et al* 1998 *Phys. Rev. Lett.* **80** 724-27
[21] Okamura S. *et al* 2004 *Nucl. Fusion* **44** 575-81
[22] Henneberg S.A. 2019 *Nucl. Fusion* **59** 026014
[23] Xu Y. 2016 *Matter Radiat. at Extremes* **1** 192-00
[24] Nelson B.E. *et al* 2003 *Fusion Eng. Des.* **66-68** 169-174
[25] Zarnstorff M.C. *et al* 2001 *Plasma Phys. Control. Fusion* **43** A237–A249
[26] Li Yang, Liu H, et.al 2020 *Plasma Phys. Control. Fusion (submitted)*
[27] Merkel P. 1987 *Nucl. Fusion* **27** 867

[28] Strickler D. J. *et al* 2002 *Fusion Sci. Technol.* **41** 107-115
[29] Zhu C. *et al* 2018 *Nucl. Fusion* **58**
[30] Sinha P. *et al* 2019 *Nucl. Fusion* **59** 126012
[31] Dinklage A. *et al* (W7-X Team) 2018 *Nat. Phys.* **14** 855
[32] Hirshman S.P. 1983 *Phys. Fluids* **26** 3553-0
[33] Kishimoto Y. 1999 *Plasma Phys. Control. Fusion* **41** A663-78
[34] NEILSON, G. H. *et al* 2000 *Phys. Plasmas* **7** 1911
[35] Akihiro Shimizu. *et al* 2003 *Fusion Eng. Des.* **65** 109-118
[36] Matt Landreman. *et al* 2017 *Nucl. Fusion* **57** 046003 (15pp)
[37] Spitzer L. 1958 *Phys. Fluids* **9** 130-41
[38] Mercier C. 1964 *Nucl. Fusion* **4** 213-26
[39] Hudson S. R., Startsev E., and Feibush E. 2014 *Phys. Plasmas* **21** 010705
[40] Pfefferl´e D., L. Gunderson, Hudson S.R., and Noakes L. 2018 *Phys. Plasmas* **25** 092508
[41] Hegnal C.C. and Hudson S.R. 2001 *Phys. Rev. Lett.* **87(3):**035001
[42] Nemov V.V. *et al* 1999 *Phys. Plasmas* **6** 4622
[43] Matsuoka K. *et al* 1988 (IAEA, Vienna) Vol.2 *Plasma Phys. Control. Fusion* **p.411**
[44] Isobe M. *et al* 2002 *Plasma Phys. Control. Fusion* **44** 5A
[45] Nemov V.V. *et al* 2003 *Plasma Phys. Control. Fusion* **45** 43-52
[46] Heyn M.F. *et al* 2001 *Plasma Phys. Control. Fusion* **43** 1311–1324
[47] Turkin Y. *et al* 2011 *Phys. Plasmas* **18** 022505
[48] Sanchez R. *et al* 2001 *Plasma Phys. Control. Fusion* **43** A237-49
[49] Vernon Wong H. *et al* 2001 *Phys. Plasmas* **8** 2415
[50] Ware A.S. *et al* 2002 *Phys. Rev. Lett.* **89** 125003
[51] Okamura S. *et al* 2020 *J. Plasma Phys.* **86**, 815860402
[52] Sunn Pedersen, T. *et al* 2016 *Nat. Commun.* **7** 13493
[53] Hammond K.C. *et al* 2019 *Plasma Phys. Control. Fusion* **61** 125001 (19pp)
[54] Asakura N., Hosogane H., Tsuji-iio S., Itami K., Shimizu K., and Shimada M. 1996 *Nucl. Fusion* **36** 795
[55] Soukhanovskii V.A. *et al* (the NSTX research team) 2005, J. *Nucl. Mater.* 337–339 475
[56] Liu S.C. *et al* 2014 *Phys. Plasmas* **21** 022509
[57] U. Stroth, M. Murakami, R.A. Dory et al 1996 Nucl. Fusion **36**,1063